Challenges in Three-Dimensional Printing of High-Conductivity Copper

Tahany I. El-Wardany[1]
United Technologies Research Center (UTRC),
East Hartford, CT 06108
e-mail: elwardti@utrc.utc.com

Ying She
United Technologies Research Center (UTRC),
East Hartford, CT 06108

Vijay N. Jagdale
United Technologies Research Center (UTRC),
East Hartford, CT 06108

Jacquelynn K. Garofano
United Technologies Research Center (UTRC),
East Hartford, CT 06108

Joe J. Liou
United Technologies Research Center (UTRC),
East Hartford, CT 06108

Wayde R. Schmidt
United Technologies Research Center (UTRC),
East Hartford, CT 06108

With recent advancements in additive manufacturing (AM) technology, it is possible to deposit copper conductive paths and insulation layers of an electric machine in a selective controlled manner. AM of copper enables higher fill factors that improves the internal thermal conduction in the stator core of the electric machine (induction motor), which will enhance its efficiency and power density. This will reduce the motor size and weight and make it more suitable for aerospace and electric vehicle applications, while reducing/eliminating the rare-earth dependency. The objective of this paper is to present the challenges associated with AM of copper coils having 1 × 1 mm cross section and complex features that are used in producing ultra-high efficiency induction motor for traction applications. The paper also proposes different approaches that were used by the authors in attempts to overcome those challenges. The results of the developed technologies illustrate the important of copper powder treatment to help in flowing the powder easier during deposition. In addition, the treated powder has higher resistance to surface oxidation, which led to a high reduction in porosity formation and improved the quality of the copper deposits. The laser powder direct energy deposition (LPDED) process modeling approach helps in optimizing the powder deposition path, the laser power, and feed rate that allow the production of porosity free thin wall and thin floor components. The laser powder bed fusion (LPBF) models identify the optimum process parameters that are used to produce test specimens with >90% density and minimum porosity.
[DOI: 10.1115/1.4039974]

1 Introduction

A wide range of additive manufacturing (AM) processes for depositing metals exist with varying attributes in terms of precision, integrity and microstructure, material properties, cost, etc. The selection of the proper AM process is based on the application, including considerations of material type, part size, complexity, process availability, level of inspection, and validation. The geometric freedom of some AM processes is still somewhat restricted by the need to provide and remove support structures and the difficulties associated with removing the unsolidified material contained in part cavities [1–5]. Three-dimensional (3D) printing of components from pure copper or copper alloy [6,7] is spurring a wide range of applications including high-efficiency electric machines. However, some of the pure copper properties present significant processing challenges in this case. Pure copper has a relatively high thermal conductivity, which rapidly conducts heat away from the melt area resulting in high local thermal gradients. This can lead to layer curling, delamination, and build or part failure. Additionally, copper's high ductility hinders post-build powder removal and recovery. Copper particles also tend to agglomerate, reducing overall flowability and impeding powder deposition. In addition, copper is sensitive to oxidation, which requires a special handling and storage of it before, during, and after part fabrication.

Research available in the open literature concentrates on experimental optimization of the process parameters for processing copper using electron beam manufacturing ARCAM (EBM) [8]. Results showed high-density parts can be made from oxygen-free, high-conductivity (OFHC) copper. However, EBM beam size is quite large (~0.5 mm) compared to the laser spot size in laser-directed energy deposition or laser powder bed fusion (LPBF) AM processes. This will limit the fine features size that can be produced (Fig. 1). In addition, the production of part with high surface roughness requires a post processing, which may not be applicable for producing electric machine coils and insulations. Moreover, columnar arrays microstructure is observed for deposited copper samples with orthogonal interruptions of the columnar arrays as a consequence of beam scan anomalies [9].

The deposition of OFHC copper via laser additive manufacturing (LAM) is not as advanced as EBM due to its high reflectivity

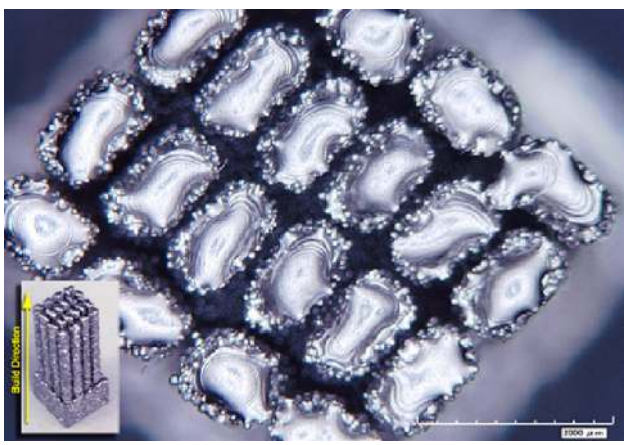

Fig. 1 Electron beam manufacturing deposited wire of 0.5 × 0.5 mm cross section representing on induction motor coil design [9]

[1]Corresponding author.
Contributed by the Electronic and Photonic Packaging Division of ASME for publication in the Journal of Electronic Packaging. Manuscript received October 9, 2017; final manuscript received April 13, 2018; published online May 9, 2018. Assoc. Editor: Kaushik Mysore.

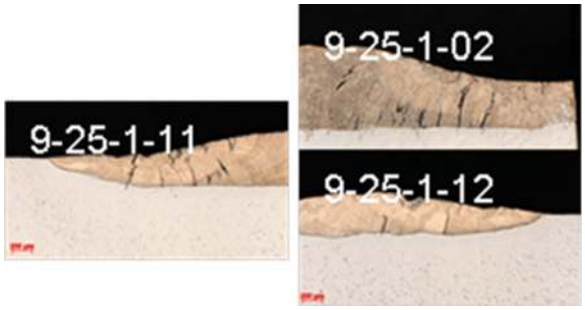

Fig. 2 Laser powder depositions of copper layers with extensive cracking at the interface

Fig. 3 Laser powder depositions of copper at different process parameters and porosity density

and high thermal conductivity (thus low absorptivity). Because of these properties, solidification cracking and porosity are always observed when depositing copper using LAM [6–8]. Copper powder particle morphology, insufficient energy, and thermal history have a great influence on cracking and porosity defects as shown in Figs. 2 and 3.

For LAM, high power and low deposition speed are needed to successfully deposit pure copper while maintaining physical and mechanical properties of the copper within acceptable levels. This paper discusses several approaches that are used to ensure sustainable deposition of OFHC copper powder to fabricate induction motor coils. Copper powder surface treatment was used to reduce the generation of copper oxides on the powder surface. In addition, physics-based models were developed for both laser powder deposition process and laser powder bed fusion process. The models were then used to determine the optimum process parameters for crack free and minimum porosity deposits. Details of the three approaches will be discussed in Secs. 2–4.

2 Copper Powder Treated by Fluidized Bed

Laser powder direct energy deposition (LPDED) of copper has been challenging due to high levels of porosity in the resulting builds (Fig. 3). It has been speculated that the observed porosity is caused by residual oxides, both internal and on the surface of the feedstock powder. Internal oxides can be mitigated through proper selection of the powder production process. Inert gas atomization is the preferred technique, resulting in powders with negligible oxygen content in the interior. Surface oxides, however, pose a complicated issue. As powders are exposed to atmosphere during transport and storage, an oxide layer will grow on the surface. This is unavoidable unless the powder is kept in inert conditions for the entirety of its life. While possible, it is not feasible to prevent all oxide contamination on the powder surface. It is possible to

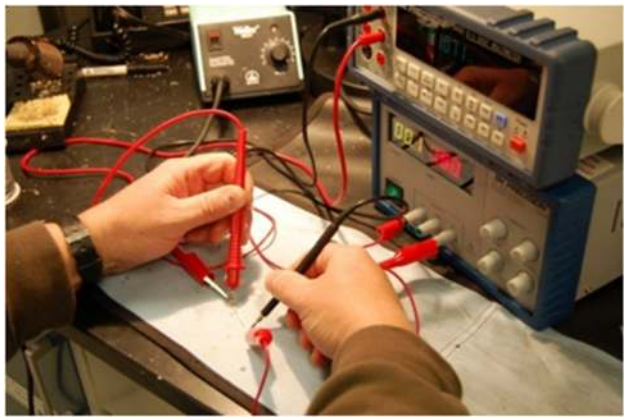

Fig. 4 Four points probe conductivity measurement

remove this surface oxide, by heating powders in a reducing environment (typically forming gas comprised of argon + hydrogen). Once the oxide is removed, again the issue of preventing re-oxidation is a concern.

Three possible strategies for mitigating the concerns of oxides present in copper powders for AM were proposed as follows:

(1) Use of reducing gas environment during LPDED AM;
(2) Use of alternative copper alloys with lower sensitivity to oxides;
(3) Protection of powders.

The first option, which employs reducing gas in the LPDED system, will allow for the powder carrier gas to be fed from a premixed gas cylinder of 4% hydrogen in argon forming gas. This is a common gas used for the reduction of materials in a furnace. The second option, alternative copper alloys, was investigated by studying addition of alloying elements to copper to eliminate porosity due to copper oxides. Careful selection of an alloying element for the copper feedstock could produce copper part with minimum porosity. However, care must be taken in selecting the alloy, as the conductivity of copper is easily degraded with addition of alloying elements.

In Ref. [10], Fig. 2.1.1 demonstrates the sensitivity of copper to alloying elements. This figure indicates that the three materials least detrimental to conductivity include silver, cadmium, and zinc. The high cost of silver makes it less suitable; however, a prospective feedstock powder was identified. ECKA Granules (Germany) has available silver-coated copper material (Sil-Shield). This silver coating would provide two benefits: protection of the copper from oxidation and an added alloy element to potentially reduce porosity while minimally impacting electrical conductivity.

An experimental batch of mechanically alloyed 3% zinc–copper powder was procured. The milling agent was removed from the powder, to avoid issues during LPDED. Single wall and columnar structures were built for testing. Electric conductivity was measured to be 97% using four points probe conductivity measurement system shown in Fig. 4. The computerized axial tomography scanning of the samples illustrated a reduction in the internal porosities. In addition, protection of powders from oxidation was also explored through developing a number of technologies for both cleaning powders as well as protecting them from atmospheric concerns.

The formed copper oxides on the powder surfaces are detrimental to the quality of the deposits made by laser powder based additive manufacturing techniques, in particular, for electrical conduction applications. The electrical conductivity of copper decreases significantly with impurity content of oxygen. In addition, the copper oxides on the surfaces of the copper powder cause the porosity in the deposits. The oxides decompose into copper

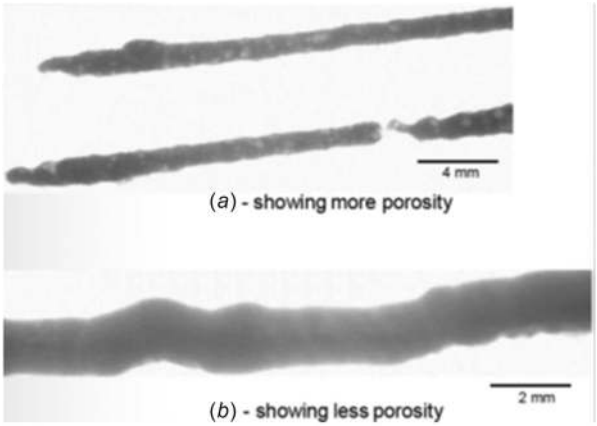

Fig. 5 Real-time X-ray image of LPDED deposit with uncoated (*a*) and coated (*b*) copper powder

and oxygen gas during the laser processing. As a result, the released oxygen can cause rapid expansion, contributing porosity formation in the deposit.

One effective and potential solution to overcome that issue is to reduce the copper oxides on the copper powder to metallic copper through surface treatment of the copper powder using a fluidized bed method developed and detailed elsewhere [11]. Copper powder was reduced by hydrogen gas first and then treated by coating a very thin layer (a few nanometers) of polydimethylsiloxane in the lab rig [11]. The thin layer of polydimethylsiloxane on the coated copper powder was vaporized away before the copper powder reached the melt pool during the LPDED process. Two copper deposit samples (~50 mm long and 1.6 mm in diameter) were made by a LPDED process using the untreated and treated copper powders. Real-time X-ray images of the deposits showed clearly that the deposit with the uncoated powder exhibited more porosity (Fig. 5(*a*)) than that derived from the coated powder (Fig. 5(*b*)). This demonstrated that the developed technology [11] can reduce the oxides on the surfaces of copper powder, thus improving the quality of the copper deposits.

In addition, the treated copper powder demonstrated significantly higher oxidation resistance. Figure 6(*a*) shows the photo images of the untreated and treated copper powders taken later after the treatment. The treated copper powder still showed a color typical of metallic copper metallic while the untreated powder exhibited the color of oxidized copper, indicating the oxidation resistance of the treated powder.

The morphology of copper powder plays an important role in the formation of porosity [12,13]. It is preferable that the copper powder has spherical shape. A design of experiment (DOE) has been conducted to observe the formation of porosity. This DOE focuses on the powder type, laser power, laser head, and powder feed rate. Table 1 shows the parameters used for this DOE.

It is found from the DOE results that powder type and laser power are the most significant parameters related to the formation of porosity. The X-ray images for the formation of porosity are shown in Fig. 6(*b*). The DOE conclusions are as follows:

- Copper powder treatment is used to ensure better flow of the powder from the nozzle during the deposition (flowability). The powder tends to adhere to each other and to the nozzle surface which reduce the powder deposition rate or stop the powder flow from the nozzle.
- The treated powder has minimal porosity when the laser power is low; however, several huge pores were unexpectedly formed when the laser power is equal to or greater than the intermediate laser power. This strongly indicates that the treatment alters the material thermophysical properties and interaction with the laser beam.

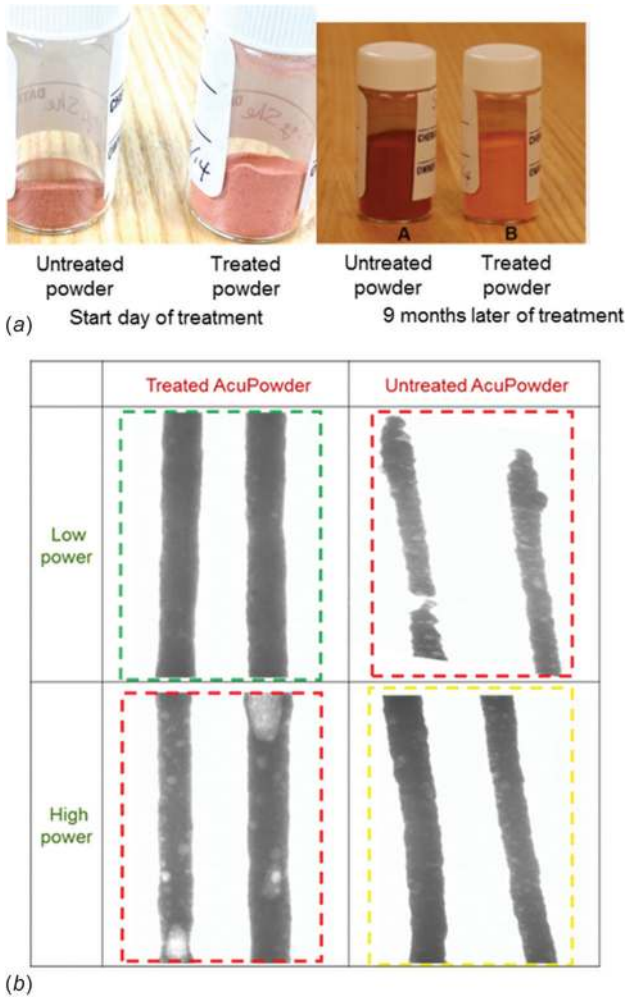

Fig. 6 (*a*) Photo images of the untreated (A) and treated (B) copper powders taken at the start day of treatment and 9 months later after the treatment and (*b*) treated copper powder increased flowability and reduced required laser power [11]

Table 1 Parameters used for the DOE

Powder	Treated and untreated AcuPowder copper powder
Deposit shape	Column
Substrate	25.4 × 25.4 × 1 mm copper
Initial substrate temperature	293 K
Laser head speed	1.905 mm/s
Laser head	Standard and high over hang
Constant laser power (W)	High = 406
Powder feed rate base on untreated powder (mm^3/s)	High = 23

- The untreated powder has high porosity and even hot cracking when lower power is used and low porosity when the high laser power is used.

3 Physics-Based Modeling of Laser Powder Direct Energy Deposition Process

The main objective in modeling LPDED process is to define the process parameters for copper deposition that initiate minimum distortion and porosity. The modeling of LPDED process is conducted mainly using the program simulation of additive

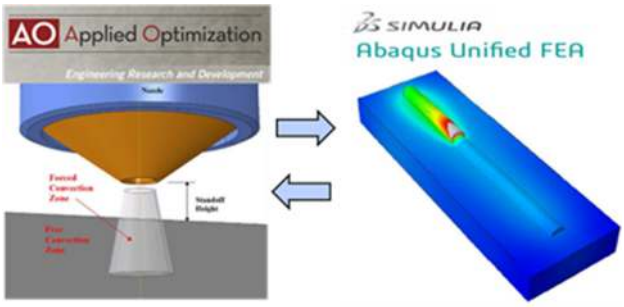

Fig. 7 Simulation of additive manufacturing processes setup [14]

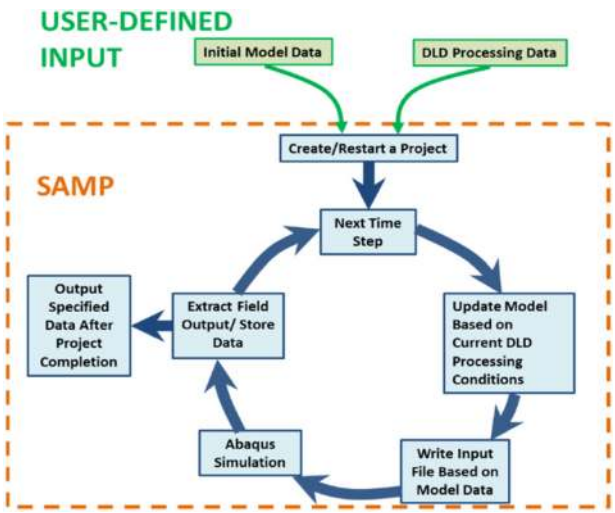

Fig. 8 Simulation process flow [14]

manufacturing processes (SAMP), Applied Optimization, Inc. (Dayton, OH) [14]. SAMP is able to automatically create time series, step-by-step models of the process. SAMP provides the preprocess and postprocess data for Dassault Systemes ABAQUS [15,16], a finite element analysis program, to execute thermal and stress simulations as shown in Fig. 7.

The simulation process of LPDED process is depicted in Fig. 8. The first step in the simulation is the user-defined input. Two groups of data are in the user-defined input: (1) initial model data that includes 3D deformable solid part, deposit eligible surface, and mesh in the substrate; and (2) design of laser deposition that includes schedule, tool, additive manufacturing process items, constants, and simulation parameters.

A project file is formed from the user-defined input. SAMP then breaks the total analysis of laser deposition into times steps. In each time-step, SAMP builds the deposit to be added.

Figure 9 shows the results obtained by the authors for one example of the temperature distribution in Kelvin during the copper deposition. The square copper prisms are deposited on the substrate from the bottom to the top. The cross-sectional dimension of the prism is 1 mm by 1 mm. The laser beam power, scan velocity, and powder volume rate are, respectively, 1250 W, 6.25 mm/s, and 9.89×10^{-9} m^3/s. Figure 10 shows the results obtained by the authors for predicting residual stress distributions for the whole model and selected surface sets. Figure 11 shows the prediction of copper distortion during deposition obtained from the models developed by the authors. Table 2 illustrates three different processes and corresponding parameters that will be modeled using SAMP. The material properties used for these three processes are based on the properties of pure copper C11000. The properties of pure copper C11000 will be close to those of untreated copper powder mentioned earlier. For treated copper powder, no measurement of thermophysical properties has been provided. However, a sensitivity analysis was conducted to study the influence of copper's thermophysical properties on the LPDED process.

The process parameters considered here are initial substrate temperature, laser power, scan speed, and powder feed rate. The ambient temperature at 293 K is considered for the three methods. Sciammarella et al. [16] reported that the first deposited copper layer on a steel substrate can be done using 700 W of laser power. Therefore, process (I) intentionally simulates the first deposited layer on the copper substrate using constant laser power of 700 W. For process (I), Fig. 12 shows the temperature distributions when the laser head moves to the midpoint and the end of the deposit line, respectively. The constant laser power and maximum temperature as a function of deposit time are depicted in Fig. 13-process (I), where the maximum temperature gradually increases with time. The temperature is less than the solidus point of pure copper. Therefore, process (I) does not provide sufficient laser power to allow diffusion of copper powder into the substrate, leading to hot cracking [12,16,17].

In order to improve the insufficient laser power condition in process (I), process (II) utilized an algorithm-controlled laser power built in SAMP software for the deposit process. The

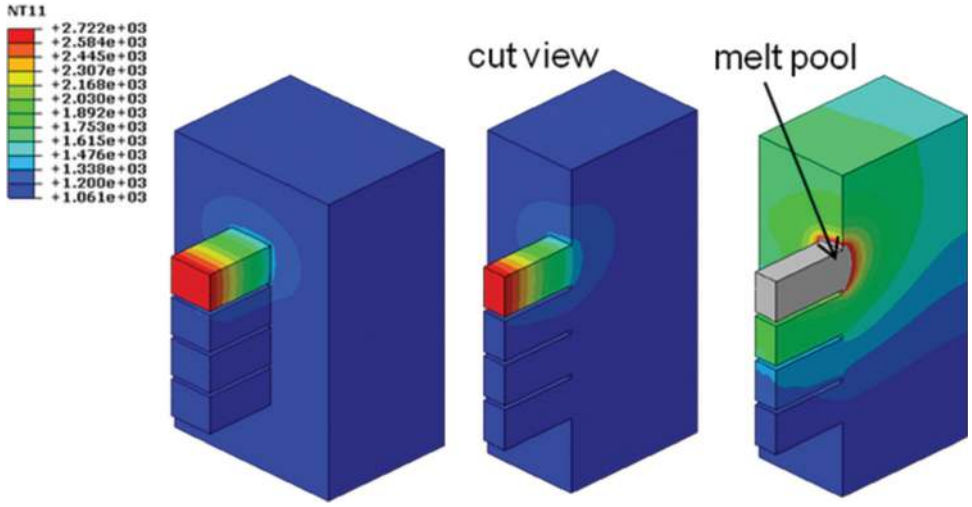

Fig. 9 Temperature distributions during copper deposition

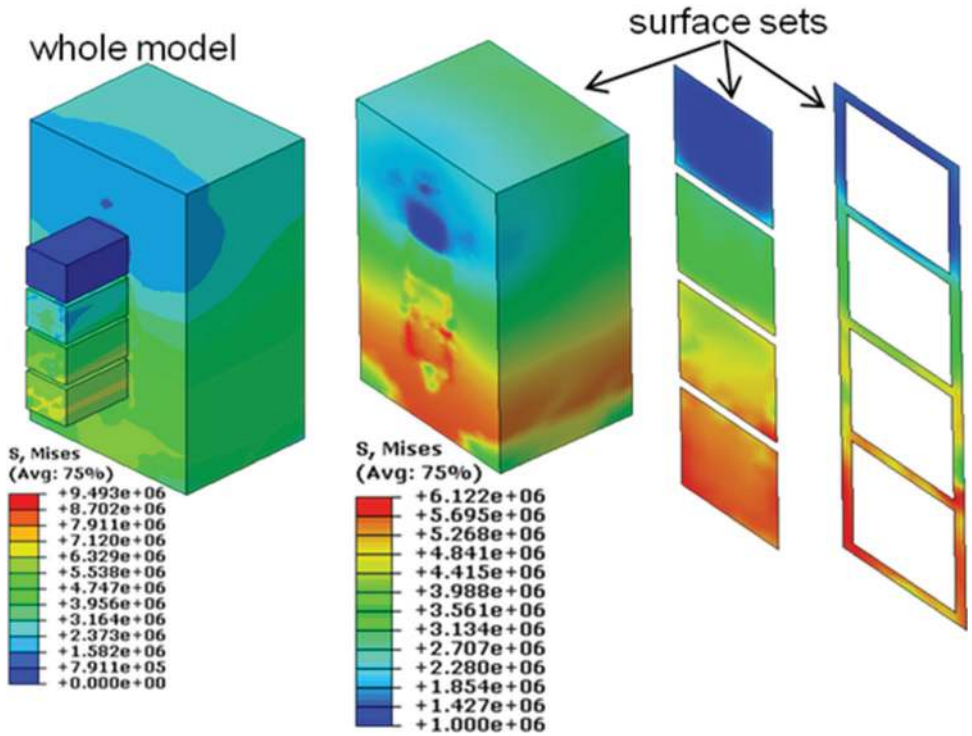

Fig. 10 Residual stress distributions after copper deposition

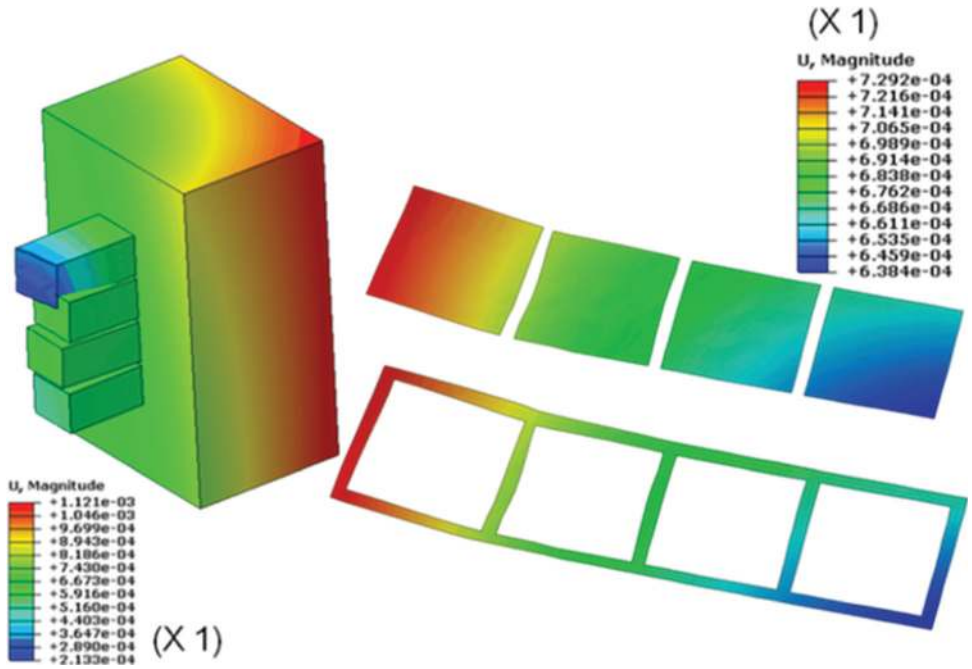

Fig. 11 Distortion of substrate and the square copper prisms during deposition (models developed by the authors using a licensed SAMP code)

Table 2 Process parameters for the first deposited layer of C11000

Method	Substrate initial temperature (K)	Laser power (W)	Laser travel speed (mm/s)	Powder feed rate (mm^3/s)
Process (I)	293	700	2.1	2.99
Process (II)	600	850 (initial), modified by algorithm for temperature optimization	2.1	2.99
Process (III)	600	1000 (dwelling) controlled	2.1	2.99

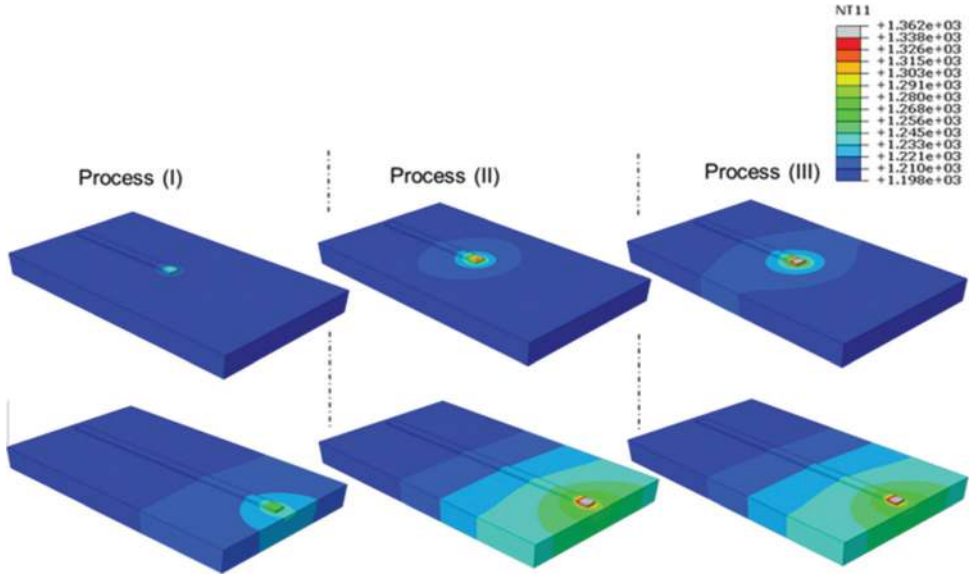

Fig. 12 Temperature distributions for various process methods

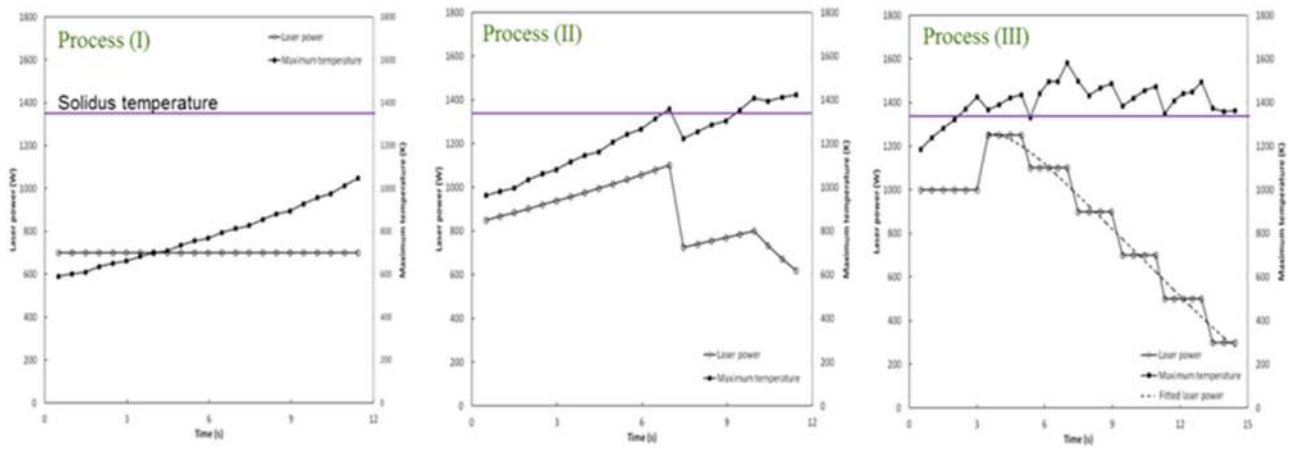

Fig. 13 Laser power and maximum temperature as a function of time for various process methods

algorithm is used to adjust the laser power for the next time-step based on the average temperature in the melt pool at the current time-step. In other words, if the calculated average temperature in the melt pool of the current time-step is out of the user-defined criterion, the laser power in the next time-step will be adjusted. The adjustment ratio is defined as the ratio of the new laser power to the previous step's power value. Adjustment ratio is scaled by a multiplier which determines the aggressiveness of the laser adjustment scheme. In process (II), the temperature range between 1200 and 1300 K is used for the user-defined criterion based on the preliminary analysis conducted earlier to ensure the diffusion of the copper powder. In addition, the initial substrate temperature is changed to 600 K. The substrate preheat is kept constant during the deposit process.

Figure 12 process (II) shows the temperature distributions when the laser head with a constant power moves to the mid-point and the end of the deposit line, respectively. The algorithm-controlled laser power and maximum temperature as a function of deposit time are depicted in Fig. 13-process (II). In the beginning time-step, the initial laser power, 850 W, provides insufficient energy to melt the powder; therefore, the laser power is increased 2% in the next time-step. This time-increasing laser power is continued until the maximum temperature reaches 1359 K at $t = 6.96$ s, and then the laser power is reduced to avoid overheating the deposit and substrate. When the algorithm detects the temperature is less than the user-defined criterion, it increases the laser power again to provide sufficient energy for the deposition. Generally speaking, process (II) improves the cladding bonding with 20% of cladding length reaching the solidus temperature.

To further improve the interface bonding in the initial half deposit, a heating-dwell step is added in process (II) to optimize the deposit process. The initial substrate temperature is same as process (II) at 600 K. In the heating-dwell step, a higher laser power of 1000 W is applied to heat the substrate at the starting point of deposit for 3 s so that a melt pool will be formed on the substrate surface. This step does not deposit powder; therefore, the whole laser power is applied on the substrate without the shadow effect. The laser power is then increased to 1250 W and kept for 2 s. The laser power is further reduced to 1100 W and stepwise reduced with 200 W of reduction for an interval of 2 s until a full cladding length is completed. Details of laser power schedule can be seen in Fig. 12-process (III). The maximum temperature history during the whole cladding for process (III) is also depicted in Fig. 12-process (III). It is evident that process (III) significantly improved the cladding bonding with 80% of cladding length reaching the solidus temperature. In Fig. 13-process (III), a

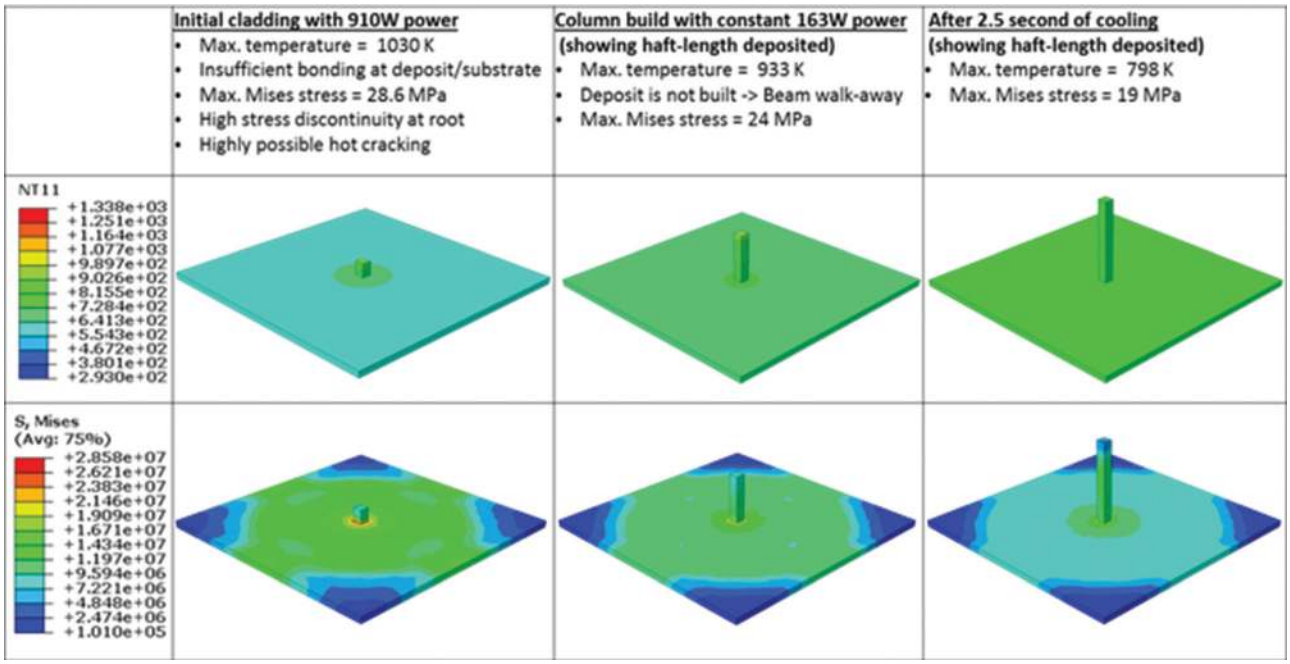

Fig. 14 Model predicts insufficient laser power for the diffusion for untreated powder

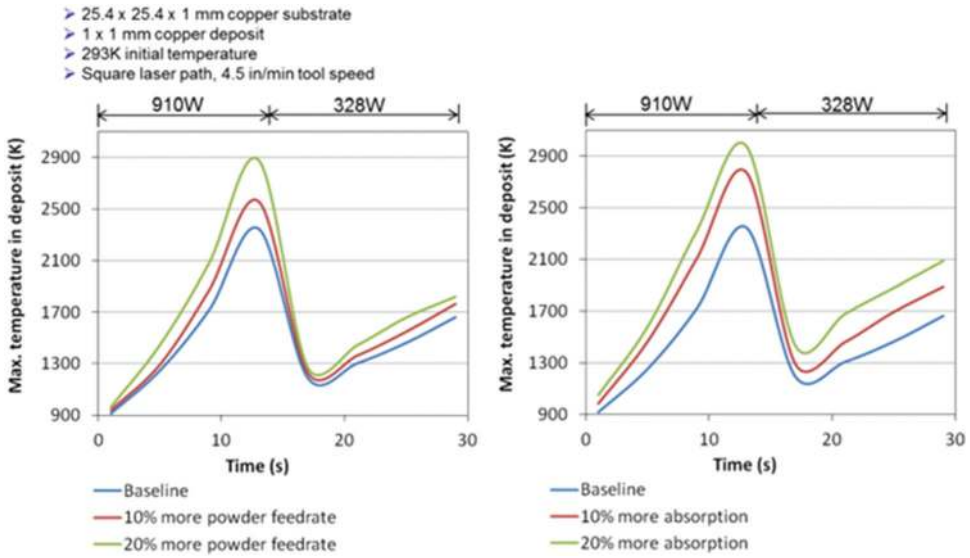

Fig. 15 Powder feed rate and absorption coefficient positively affect the temperature rise in deposition

fitting curve of laser power is also plotted for the stepwise laser power, which represents a more practical condition (time-varying laser power) should be used for the first layer of deposit.

Figure 14 shows a simulation for the untreated powder. The model predicts that the laser power was insufficient to deposit copper on copper. The model was stopped and the copper build was not completed when the laser was allowed to heat the substrate for 2.5 s before building the specimen the model completed the copper build.

3.1 Sensitivity Analysis. As indicated in Sec. 3, the treated copper powder alters powder flowability and thermophysical properties [11]. It is difficult to measure these changes. A sensitivity analysis is conducted for column builds to examine the temperature of deposit.

This analysis focuses on the powder feed rate and laser absorption by increasing 10% and 20% nominal values with respect to the pure copper ones. Figure 15 shows that both powder feed rate and absorption coefficient positively increase the maximum temperature in the deposit process.

4 Powder Bed Process Development for Copper Deposition

Laser absorption is typically higher in a powder bed than in solids due to multiple reflections and absorptions of the laser between powder particles in the powder bed. For copper, absorption of Nd:YAG laser ($\lambda = 1064$ nm) is reported to increase from ~2–5% at room temperature to ~59% [18,19]. This significantly

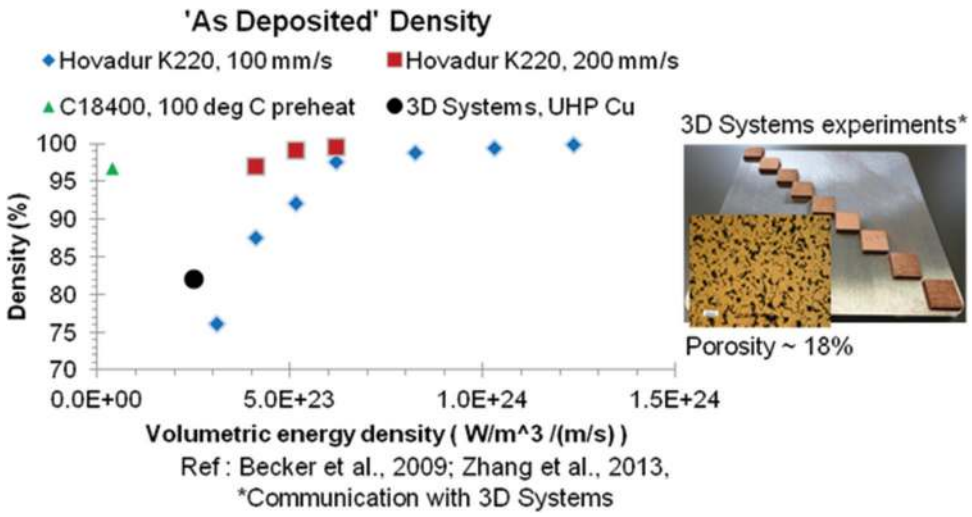

Fig. 16 As deposited density of some copper alloys (from open literature) as a function of volumetric energy density (left). Cross section of deposited sample showing lack of fusion porosity defect (right).

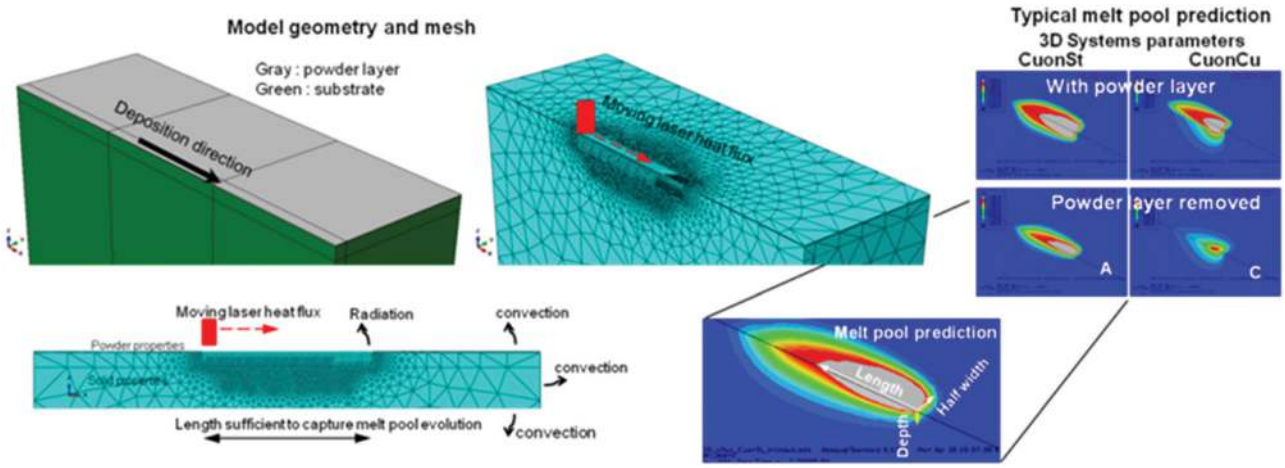

Fig. 17 Half model geometry and finite element mesh (top left) utilized for powder bed fusion single track melt pool modeling with some thermal boundary conditions (bottom left). Melt pool results are shown for 3D systems initial process parameters (right).

reduces the energy required to melt the same amount of material. Due to a smaller laser spot size and smaller layer thickness, typically used in the powder bed process, geometric resolution is better than in a typical powder deposition process (e.g., LPDED process), helping to achieve better surface features. Powder bed process was developed to deposit electric machine copper coils.

Currently, there is limited data available in the open literature on laser powder bed deposition of copper, and most of the work is on the deposition of copper alloys [20,21] (rather than pure copper) on steel (as opposed to copper) substrates, typically used for injection molding tool inserts to efficiently carry heat away from the hot-spots. These copper alloys (e.g., Hovadur® K220, C18400) have low electrical conductivity, making them of lower interest for electrical applications as in motors. Limited experiments using laser powder bed fusion process to additively manufacture of pure copper on steel substrate (referred to as "CuonSt" in this paper) were performed, and these early trials showed ~18% porosity in the deposited material, which appeared to be mostly due to "lack of fusion" porosity defects (Fig. 16, right). A model was developed for the powder bed fusion single track melt pool to guide the copper on copper (referred to as "CuonCu" in this paper) deposition process.

The single track melt pool model is a finite element-based thermal model implemented in ABAQUS general purpose finite element software. In the model, a powder layer is modeled as a continuum layer with equivalent material thermophysical properties, taking into account initial and reduction in porosity of the powder bed during the melting process. The laser is modeled as a heat source with volumetric heat flux definition which travels into the powder bed with a prescribed laser scanning velocity (refer Fig. 17). The definition of heat flux is a function of many factors including power distribution within laser beam, material laser absorption co-efficient, laser optical penetration depth into the powder bed (function of material and particle size distribution), and powder bed thickness. The substrate is modeled as a solid with appropriate temperature-dependent thermophysical properties. Figure 17 shows the geometry and finite element mesh utilized in the analysis, as well as some thermal boundary conditions. Taking advantage of the symmetry of the problem about the laser travel center line, only half of the geometry is modeled in the analysis.

Melt pool modeling results show temperature distribution in the powder and the substrate with the melt pool region shown in gray color. Only half of the melt pool is shown, as results are symmetric about the laser travel center line, as noted earlier. Melt pool

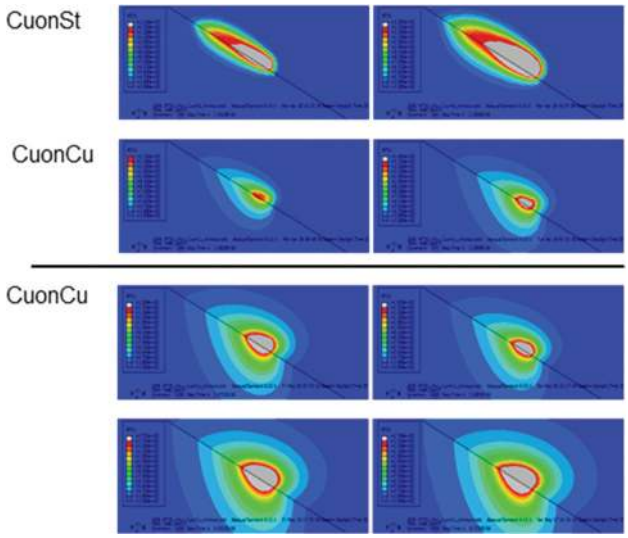

Fig. 18 Melt pool model results

predictions, shown in Fig. 17, are for default process parameters (laser power = 180 W, scanning speed = 2800 mm/s) that resulted in ~18% porosity (or 82% density). As can be seen in Fig. 17, the default parameters—while providing some substrate melt pool and wetting on steel substrate (A)—provide almost no substrate melt pool when the substrate material is changed to copper (C). These results also point to a key source of lack of fusion porosity defects observed in their build. In the first set of experiments, specific energy input is increased by maintaining or increasing laser power while reducing the scanning speed. As can be seen in Fig. 16, with higher energy input "as deposited density" increased from below 85% to greater than 95% (although results are for copper deposition on steel substrate).

Using melt pool modeling, a laser power and scanning speed design DOE is created. Increasing laser power and volumetric energy density is kept as a goal, which is substantiated by melt pool modeling results of increased substrate penetration (see Fig. 18). Combinations of nine DOE points (variables are laser power and scanning speed) are created separately for copper on steel as well as copper on copper deposition. Figure 19 shows both the builds. Deposited sample geometries contain specimen for density and electrical conductivity measurements as well as few "bridge" shapes loosely representing end turn geometry. The purpose of these "bridge" geometries is to check the feasibility of depositing unsupported horizontal segments of individual strands in the end turns. Bridge geometries use a 1 mm × 1 mm cross section. Density specimens are of 1 mm × 1 mm and 6 mm × 6 mm cross section while electrical conductivity measurement specimens are of 1 mm × 1 mm in cross section and 25 mm in length. All the samples were prepared using a Phenix ProX 200 machine which has a maximum laser power of 300 W.

Figure 20 shows melt pool modeling results for some of the DOE parameters and corresponding density measurements from deposited samples. Melt pool modeling results show temperature distribution in the substrate (powder layer is removed in the visualization) with substrate melt pool shown in gray color. As can be seen in Fig. 20, all the experimental samples showed density higher than that produced with default process parameters. The maximum density obtained was ~91%. Good correlations between model predicted substrate melt pool size and measured density is observed. Measured densities also show a strong correlation with the volumetric energy density. Based on experimental observations and melt pool model results, additional process conditions which increase substrate melt pool further are proposed for the next round of development work. Metallographic cross sections were prepared to better understand process condition effects on deposit quality. All test conditions were sectioned, optically imaged, and analyzed for porosity and structure on specimens from both the CuonCu and CuonSt DOE (Fig. 20).

Figure 21 shows transverse cross sections on 1 mm × 1 mm test specimens plotted as a function of laser power and laser speed for the CuonCu DOE test points. Observations and image analysis data confirm density measurements indicating that increased power is effective at reducing porosity while the effect of speed is not as apparent. A high degree of surface roughness and porosity is observed on edges of all the DOE conditions and most likely due to a lack of a contour scan in the specimen build. Physical measurements showed the dimensions to be oversized by approximately 0.25 mm in both the x and y build directions.

Examination of the DOE test points in the longitudinal direction reveals significantly more information about the type of porosity in the deposit. Figure 22 shows DOE test conditions 2, 4, and 9, representing a range of process extremes, sectioned and examined across the length. The primary defect still appears to be a lack of fusion with a flattened morphology that lines up with the layering strategy of the build (defect pitch is approximately twice the layer thickness). As seen in the Fig. 22, the amount of lack of fusion decreases with increasing melt pool size. Higher magnification images for DOE# 2 samples illustrate a few spherical pores more typically associated with gas evolution. The spherical porosity is a very small fraction of the overall porosity and is also very small in size.

Larger test bars produced at 6 mm × 6 mm were measured to have significantly higher density than the 1 mm × 1 mm. Metallographic cross section-based porosity estimation confirm lower porosity levels, 3% versus 8% measured for the same DOE test condition (9). Images in Fig. 23 confirm the measurement values with lower porosity in both the transverse and longitudinal cross section. It can be observed in the longitudinal section a possible build defect with higher amounts of lack of fusion between layers.

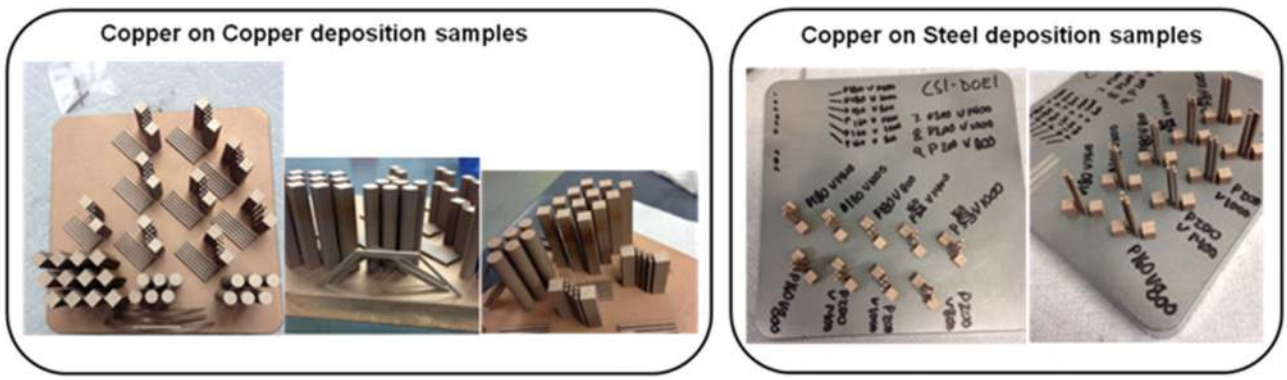

Fig. 19 Round 1: CuonCu substrate deposition samples (left) and CuonSt substrate deposition samples (right)

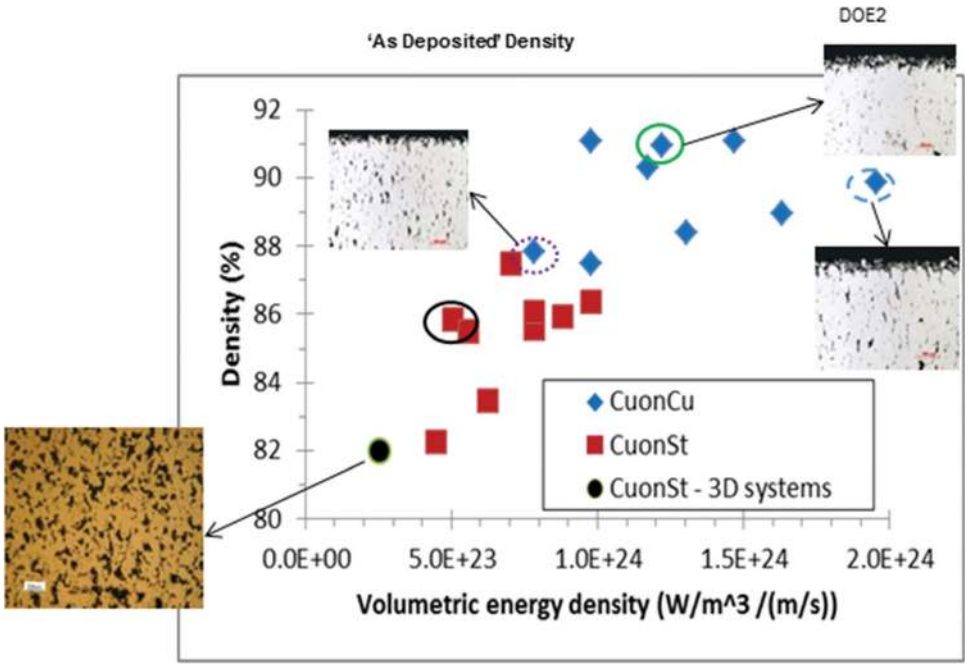

Fig. 20 Measured densities of "as deposited" samples as a function of volumetric energy density

Inquiries are in process with the Phenix machine vendor to see if this build position of the defect correlates with a measured spike in oxygen.

Electrical conductivity measurements were made on each DOE test conditions for copper on copper build and were shown to be greatly influenced by the deposit quality. Copper on steel builds is not analyzed for electrical conductivity as prior experience showed such builds show lower electrical conductivity due to iron diffusion in the copper build from the steel substrate. For copper on copper build, Fig. 24 shows a strong positive trend with increasing density on percentage International Annealed Copper Standard but shows values significantly lower than expected for porosity as the only contributor. Literature on powder metallurgy derived copper indicates a direct liner relationship between density and conductivity [22], for 90% density—the International Annealed Copper Standard should be higher versus 16% observed in the DOE test data. Literature [10] also indicates that certain impurities have a severe detrimental effect on copper conductivity.

Electron microprobe was used to determine impurities in powder used in the DOE (as received and after build) along with a test specimen. Phosphorous was measured at 0.6% in all cases,

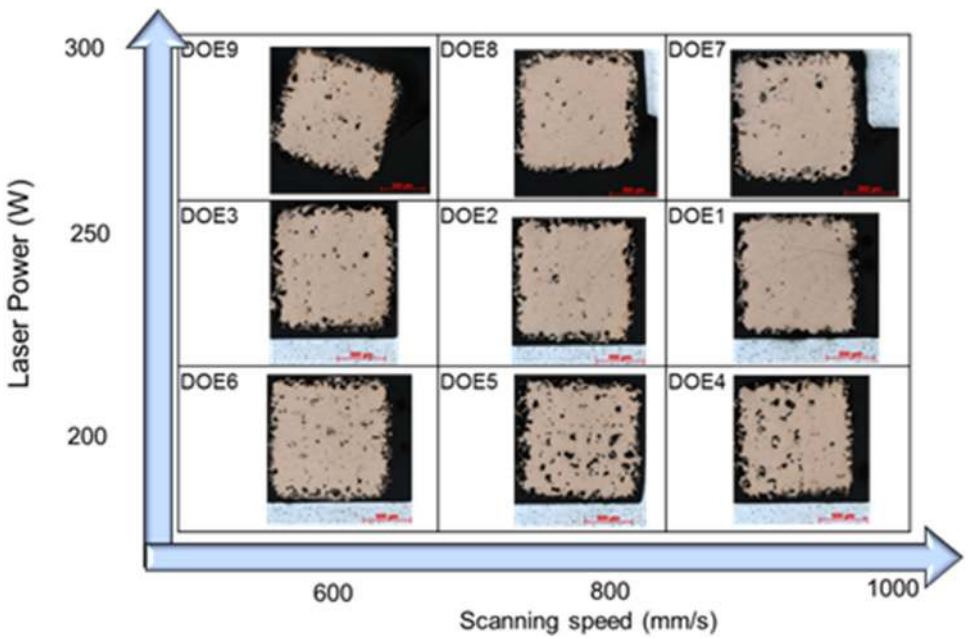

Fig. 21 Transverse metallographic cross sections for CuonCu DOE

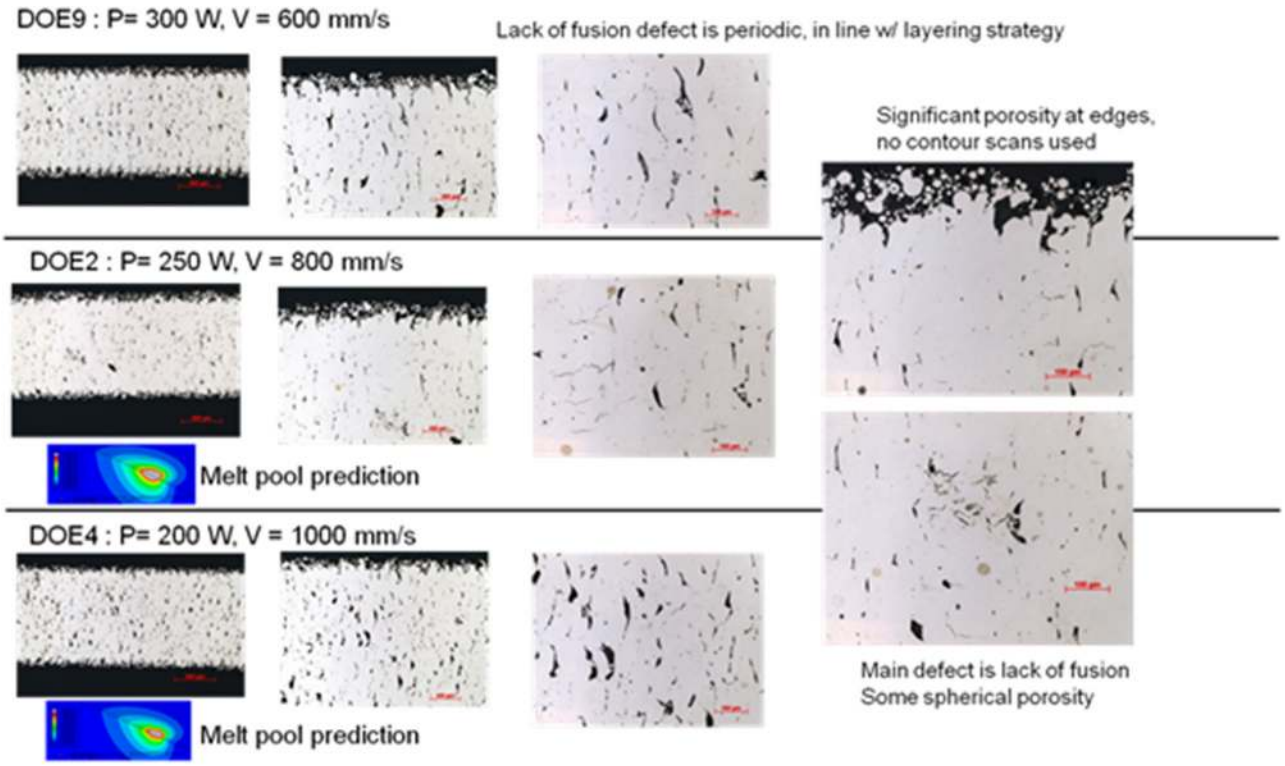

Fig. 22 Longitudinal metallographic cross sections for CuonCu DOE points 9, 2, and 4 (top to bottom)

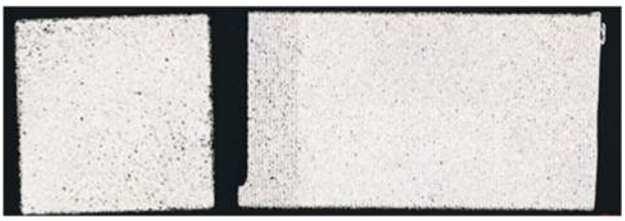

Fig. 23 Transverse (left) and longitudinal (right) metallographic cross sections for 6 mm × 6 mm CuonCu DOE point 9

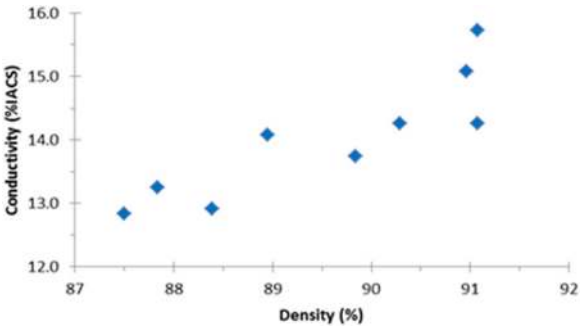

Fig. 24 Round 1 CuonCu DOE electrical conductivity as a function of density. Influence of dissolved impurity elements on the electrical conductivity of copper at ambient temperature [10].

indicating a need to better control starting powder quality and impurities. As shown in Ref. [10], this level of phosphorous would explain the drastic reduction in measured electrical conductivity.

5 Conclusion

Different approaches presented in this paper provide methods used to reduce the problems associated in additive manufacturing of OFHC copper. The potential benefits of using additive manufacturing of electric machines copper coils are to improve slot fill factor, energy density, and efficiency of an electric machine. Based on the results obtained from each approach, the following conclusions are presented:

(1) The developed copper powder treatment technique was successfully used to increase the powder flowability during laser powder deposition. The powder treatment helps in flowing the powder easier during deposition. In addition, the treated powder has higher resistance to surface oxidation and led to a high reduction in porosity formation when LPDED processing of copper thereby improving the quality of the copper deposits.
(2) The LPDED process modeling approach helps in optimizing the powder deposition scanning path, the laser power, and feed rate that allow the production of porosity free thin wall and thin floor components. The optimization method helped in increasing the copper absorption coefficient by 10–20% during deposition.
(3) The LPBF process modeling approach results in identifying the optimum process parameters that are used to produce test specimens with >90% density and minimum porosity. However, the high percentage of 0.6% phosphorous led to a reduction in the lower electrical conductivity of the copper samples produced. Authors are investigating the deposition of copper using LPBF process with OFHC copper with a phosphorous percentage less than 0.03 to enhance the conductivity.

Funding Data

- Advanced Research Projects Agency-Energy (ARPA-E) (Contract No. DE-AR0000308).

References

[1] Gideon, L., 2010, "The Role and Future of the Laser. Technology in Additive Manufacturing Environment," Phys. Procedia, **5**, pp. 65–80.

[2] Körner, C., 2016, "Additive Manufacturing of Metallic Components by Selective Electron Beam Melting—A Review," Int. Mater. Rev., **61**(5), pp. 361–377.

[3] Roy, N., Dibua, O., Foong, C. S., and Cullinan, M., 2017, "Preliminary Results on the Fabrication of Interconnect Structures Using Microscale Selective Laser Sintering," ASME Paper No. IPACK2017-74173.

[4] Rahim, K., and Mian, A., 2017, "A Review on Laser Processing in Electronic and MEMS Packaging," ASME J. Electron. Packag., **139**(3), p. 030801.

[5] O'Donnell, J., Kim, M., and Yoon, H.-S., 2016, "A Review on Electromechanical Devices Fabricated by Additive Manufacturing," ASME J. Manuf. Sci. Eng., **139**(1), p. 010801.

[6] Ramirez, D. A., Murr, L. E., Li, S. J., Tian, Y. X., Martinez, E., Martinez, J. L., Machado, B. I., Gaytan, S. M., Medina, F., and Wicker, R. B., 2011, "Open-Cellular Copper Structures Fabricated by Additive Manufacturing Using Electron Beam Melting," Mater. Sci. Eng. A, **528**(16–17), pp. 5379–5386.

[7] Ramirez, D. A., Murr, E., Martinez, E., Hernandez, D. H., Martinez, J. L., Machado, B. I., Medina, F., Frigola, P., and Wicker, R. B., 2011, "Novel Precipitate–Microstructural Architecture Developed in the Fabrication of Solid Copper Components by Additive Manufacturing Using Electron Beam Melting," Acta Mater., **59**(10), pp. 4088–4099.

[8] Frigola, P., 2008, "A Novel Fabrication Technique for the Production of RF Photoinjectors," European Particle Accelerator Conference (EPAC08), Genoa, Italy, June 23–27, Paper No. MOPP086.

[9] Center for Additive Manufacturing and Logistics, 2018, "Samples Obtained From Dr. T. J. Horn," Center for Additive Manufacturing and Logistics, Edward P. Fitts Department of Industrial and Systems Engineering, North Carolina State University, Raleigh, NC.

[10] CDA, 2018, "Select Copper Material: Composition, Purity and Alloying Elements," Copper Development Association Inc., accessed Apr. 30, 2018, http://www.copper.org/environment/sustainable-energy/electric-motors/education/motor-rotor/production/proc02/process_02_21.html

[11] She, Y., Klecka, M. A., El-Wardany, T. I., Espinal, A., Schmidt, W. R., and Dardona, S., 2013, "Particulates for Additive Manufacturing Techniques," Delavan Inc., Bamberg, SC, U.S. Patent No. 20170044354.

[12] Saprykin, A. A., Saprykina, N. A., and Arkhipova, D. A., 2016, "The Effect of Layer-by-Layer Laser Sintering on the Quality of Copper Powder Sintered Surface Layer," 11th International Forum on Strategic Technology (IFOST), Novosibirsk, Russia, June 1–3, pp. 244–246.

[13] Becker, D., and Wissenbach, K., 2009, "Additive Manufacturing of Copper Components With Selective Laser Melting," Fraunhofer ILT Annual Report, Fraunhofer-Institut für Lasertechnik ILT, Aachen, Germany.

[14] Chaudhary, A., 2010, *Metals Process Simulation* (ASM Handbook), Vol. 22B, ASM International, Materials Park, OH, pp. 240–252.

[15] Dassault Systèmes, 2014, "ABAQUS User's Manual V.6.14," Dassault Systèmes, Johnston, RI.

[16] Sciammarella, F. M., Gonser, M., and Styrcula, M., 2014, "Laser Additive Manufacturing of Copper," SME Rapid Conference on Additive Manufacturing, Detriot, MI, June 10–12.

[17] Lykov, P. A., Safonov, E. V., and Akhmedianov, A. M., 2016, "Selective Laser Melting of Copper," Mater. Sci. Forum, **843**, pp. 284–288.

[18] Glardon, R., Karapatis, N., Romano, V., and Levy, G. N., 2001, "Influence of Nd:YAG Parameters on the Selective Laser Sintering of Metallic Powders," CIRP Ann., **50**(1), pp. 133–136.

[19] Zhang, D. Q., Liu, Z. H., and Chua, C. K., 2013, "Investigation on Forming Process of Copper Alloys Via Selective Laser Melting," Sixth International Conference on Advanced Research in Virtual and Rapid Prototyping, Leiria, Portugal, Oct. 1–5, pp. 285–289.

[20] Tolochko, N. K., Khlopkov, Y. V., Mozzharov, S. E., Ignatiev, M. B., and Laoui, T., 2000, "Absorptance of Powder Materials Suitable for Laser Sintering," Rapid Prototyping J., **6**(3), pp. 155–161.

[21] Becker, D., Meiners, W., and Wissenbach, K., 2009, "Additive Manufacturing of Copper Alloy by Selective Laser Melting," Fifth International WLT-Conference Lasers in Manufacturing (LIM), Munich, Germany, June 15–18, pp. 195–199.

[22] CDA, 2018, "Characteristics and Properties of Copper and Copper Alloy P/M Materials," Copper Development Association Inc., accessed Apr. 30, 2018, http://www.copper.org/resources/properties/129_6/characteristics_properties.html